

Effects of electroporabilization and gene electrotransfert on the lateral mobility of a GPI anchored protein

Jean Michel Escoffre¹, Marie Hubert¹, Justin Teissié¹,
Marie Pierre Rols¹ and Cyril Favard²

¹ Institut de Pharmacologie et de Biologie Structurale,
CNRS UMR 5089, 31077 Toulouse Cedex, France

² Institut Fresnel, CNRS UMR 6133,
13397 Marseille Cedex, France

February 8, 2012

Abstract

Electroporabilization is a method by which molecules can be introduced in living cells through the plasma membrane. Here, we show that electroporabilization affects the lateral mobility of Rae-1, a GPI anchored protein. Our results shows that 10 to 20 % of the membrane surface is occupied by defaults or pores. Gene electrotransfert also affects the lateral mobility of Rae-1. Furthermore, we clearly show that once inserted into the plasma membrane, DNA totally excludes Rae-1, indicating that DNA molecules are tightly packed together to forms huge aggregates.

Keywords : Electroporabilization, GPI anchored, pDNA, FRAP, lateral mobility, pores.

1 Introduction

The permeability of a cell membrane can be transiently increased using an external electric field pulse. This phenomenon called electroporabilization or electroporation, lead to the formation of defaults or pores in the cell membrane [1, 2, 3]. Since this is an elegant way to introduce foreign molecules into the cytoplasm, this is routinely used in cell and molecular biology, as a very efficient way for drug, oligonucleotides and plasmids delivery

(also named electrotransfert) but also *in vivo* for clinical biotechnological applications [4, 5]. Electroporabilization occurs on different time scales:

1. *Induction step (ns)*. The field induce the membrane potential difference to increase. When it reached a critical value (about 200 mV) local defects appears.
2. *Expansion step (μs)*. Defects expand as long as the field, above the critical value, is present.
3. *Stabilisation step (ms)*. As soon as the field intensity is lower than the critical value, a stabilisation process takes place within a few milliseconds, which bring the membrane to the "permeabilized state".
4. *Resealing step (s, min)*. A slow resealing of the defaults is then occurring.
5. *Memory effect (h)*. Some changes in the membrane properties remained present on a longer time scale but the cell behavior is finally back to normal.

If kinetic of electroporabilization seems well established, very few is known about what is really occurring in the cell and its membranes at the molecular levels [6]. Nevertheless, although structural changes in the membrane have never been directly visualized under the microscope, other techniques have been used to observe electroporabilization. These include measurements of conductivity of cell suspensions and cell pellets[7, 8, 9, 10], electrooptical relaxation experiments on lipid vesicles [11, 12], charge pulse studies on lipid bilayers [12, 13], measurements of membrane voltage on cells with potentiometric fluorescence dyes [14], and monitoring the influx or efflux of molecules, fluorescence dyes [15, 16, 17, 18, 19, 20, 21, 22].

More recently, molecular simulation showed the possibility of pore formation during the pulse and pore evolution up to μs time scale[23, 24, 25]. Finally, numerical computation of the evolution of these pores has authorized a more sophisticated, but still theoretical, description of the phenomenon [26]. Krassowka et al. predict mean size of "small" pores to be around 1 nm for 97% of them while mean size of "large" pores was around 20 nm with some of them as big as 400nm in cell pulsed with a 0.6 kV.cm^{-1} electric field.

While small molecules cross the permeabilized membrane directly mainly by post-pulse diffusion, plasmid DNA first interacts with the electroporabilized part of the cell surface resulting in the formation of localized aggregates[27]. Given the size of the DNA, if the permeabilization is due to

pores, or conducting defects, as suggested by the standard theory of electroporation, the pores must be relatively large due to (i) the relatively large size of the DNA and (ii) the large charge of DNA as dielectric exclusion must be overcome [28]. The cell membrane has a much more complex organization than a model lipid bilayer. One expects that the location of regions permeabilized to DNA will be determined not only by the local electric field but also by the local membrane composition.

In order to sense the effect of electroporabilization on the plasma membrane, in the absence or presence of pDNA, we have monitored the lateral mobility of a GPI anchored protein Rae-1 during the resealing step, by means of fluorescence recovery after photobleaching (FRAP) experiments. By measuring this mobility before and after application of a permeant electric field, we show a drastic and significant change of the half time of fluorescence recovery to higher values and of the mobile fraction to lower values, both at the pole of the cell facing anode and cathode. This effect is in favor of the creation of new obstacles (pores, defects) in the plasma membrane. We also show that when DNA plasmid is inserted into the membrane after electroporabilisation, Rae-1 is totally unable to enter the area occupied by pDNA, confirming the hypothesis that plasmid DNA is accumulated in a tightly bound manner in huge clusters.

2 Material and Methods

2.1 Expression of Rae-1 in CHO cell line

The Rae1-eGFP CHO cells have been generously made by the Dr. B. Couderc (EA3035, Institut Claudius Regaud, France). CHO cells are transfected by pDNA encoding Rae1-eGFP fusion protein (generous gift from Dr. A. Aucher and Dr. D. Hudrisier, IPBS-CNRS, UMR5089, France). The transfected cells are cultured under selective pressure with G448 ($1\mu\text{g}/\mu\text{L}$) (InvivoGen, San Diego, CA). The Rae1-eGFP expressing cells are sorted out by flow cytometry (FAScan; Beckman. Instruments, Inc. Fullerton, CA). Cells were then grown as previously described [29]

2.2 pDNA labeling for electroporabilization

4.7 kbp plasmids (pEGFP-C1, Clontech, Palo Alto, CA) carrying the green fluorescent protein gene controlled by the CMV promoter were prepared from *Escherichia coli* transfected bacteria by using Maxiprep DNA purification system (Qiagen, Chatsworth, CA, USA). They were covalently labeled with

Cy-3 fluorophore using LabelIT nucleic acid labeling kit (Mirus, Madison, WI, USA) according to their protocol.

2.3 Electroporabilization

Electropulsation was carried out with a CNRS cell electropulsator (Jouan, St Herblain, France) which delivers square-wave electric pulses. An oscilloscope (Enertec, St. Etienne, France) was used to monitor the pulse shape. The electropulsation chamber was built using two stainless-steel parallel rods (diameter 0.5 mm, length 10 mm, inter-electrode distance 5 mm) placed on a Lab-tek chamber. The electrodes were connected to the voltage generator. A uniform electric field was generated. The chamber was placed on the stage of the confocal microscope (Zeiss, LSM 510, Germany). Permeabilization of cells was performed by application of millisecond electric pulses required to transfer genes and to load macromolecules into cells. Cell viability was preserved when using millisecond pulse duration by decreasing the electric field intensity [14] and [15]. 10 pulses of 5 ms duration and 0.6 kV/cm amplitude were applied at a frequency of 1 Hz at room temperature. For plated cells, the culture medium was removed and replaced by the following buffer : 10 mM K_2HPO_4/KH_2PO_4 , 1 mM $MgCl_2$, 250 mM sucrose, pH 7.4. When electroporabilization was done in presence of pDNA, for each condition, 2 μ g of the pEGFP-C1 plasmid was used.

2.4 Fluorescence recovery after photobleaching

FRAP experiments were conducted using a Zeiss LSM-510 confocal microscope. The sequence was the following, images were acquired at 5Hz frequency using the 488 nm line of an argon ion laser at a very low power to avoid photobleaching during recording. After 50 images, two regions of interests (ROI), of 1 μ m radius each, which correspond to 0.86 μ m waist of a Gaussian beam, located in front of anode and cathode respectively, were briefly photobleached ($t < 300ms$) at maximal laser power. Fluorescence recovery was monitored by acquiring successive images during 40 s. The recovery curves were obtained by plotting the mean fluorescence intensity as a function of time in these two ROI, and were corrected for fluctuations in axial position by a third ROI located into the cell, and finally normalized to the mean value of each ROI before photobleaching. The curves were fitted using eq.1 which is a slightly modified 2D diffusion model for FRAP taking into account normalization and a mobile fraction M [30, 31]:

$$F(t) = M \sum_{n=1}^{\infty} \frac{(-K)^n}{n!} \frac{1}{1 + n + 2n \frac{t}{t_{1/2}}} + (1 - M)F_0 \quad (1)$$

This equation was used to its 20th order limited development for data fitting.

Fluorescence recoveries were acquired before and at time $30s < t < 90s$ after electroporabilization on the same sample using the same sequence. At this time t , more than 50% of the cells are still permeabilized [18].

3 Results

3.1 Effects of electroporabilisation on the mobility of Rae-1

Mobility of Rae-1 was monitored by means of FRAP experiments. Fitting of the recovery curve using equation 1 lead to determination of two different parameters which are respectively : $t_{1/2}$ the half time of recovery and M which is the mobile fraction. The first parameter is a fonction of the diffusion coefficient of Rae-1, the second one is a fonction of the number of mobile Rae-1. In order to characterize the mobility of Rae-1 molecule we decided to represent the evolution of these two parameters one as a function of the other. Figure 1 represents $M = f(t_{1/2})$ before (in red) and after (in green) electroporabilisation at the anode (part A) and the cathode (part B) of the electrodes for a set of 250 different cells. The intensity of each pixels represents the number of events belonging to each class.

From this image, it can clearly be seen that in both side of the cell facing the electrodes (anode and cathode) the mobility of Rae-1 protein is reduced after electroporabilization (M slightly decrease and $t_{1/2}$ increases). This is also shown in Table 1 using descriptive statistics. Table 1 gives mean values and standard deviations of $t_{1/2}$ and M , at the pole of the cell facing the anode and the cathode, before and after electroporabilization. Student's t-test shows that except for M values at the anode ($p < 0.2$), all the other parameters score $p < 0.001$ and can be considered as significantly different.

3.2 Effects of gene electrotransfert on the mobility of Rae-1

Gene electrotransfert is known to exhibit discontinuous labeling of the DNA at the cell surface. While observed using a photonic microscope, DNA is found as clusters close or above diffraction limit *i.e.* $200nm$. We decided to probe the size of these DNA clusters more accurately by using Rae-1

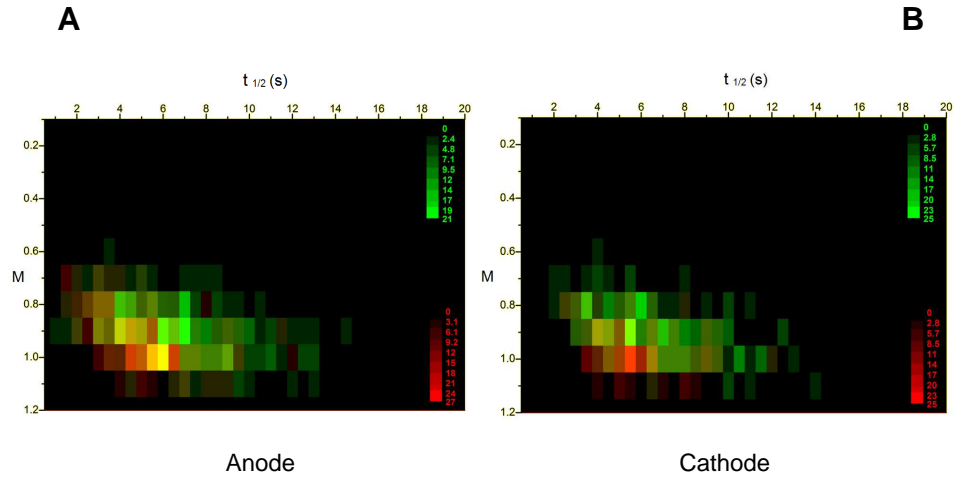


Figure 1:

Distribution of $t_{1/2}$ and M before and after electropermeabilization : M is plot as a function of $t_{1/2}$, before (in red) and after (in green) electropermeabilization for the cell pole facing the anode (part A), or the cathode (part B). Intensity scale is dispatched on the side of each image and correspond to the number of events in each class of $(t_{1/2}, M)$ couple.

Table 1: **Mean values of $t_{1/2}$ and M before and after permeabilization**

	$t_{1/2}(s)$	M
Anode		
-E	5.7 ± 2.3	0.90 ± 0.09
+E	7.2 ± 3.3	0.86 ± 0.09
Cathode		
-E	5.9 ± 2.4	0.90 ± 0.09
+E	7.2 ± 3.1	0.85 ± 0.10

dynamics. We expected a bigger effect on the reduction of mobility since this later is proportional to the size of obstacles. Surprisingly, we noticed the same effect on the mobility of Rae-1 in the absence or presence of plasmid (data not shown). Simple image analysis on cells labeled both by Rae-1 and DNA shown the absence of Rae-1 fluorescence in the DNA cluster that could account for the previous result. Nevertheless, since emission spectra of GFP widely overlap absorption spectra of Cy3, this lack in fluorescence can, oppositely, be due to a very efficient energy transfert of Förster type from Rae-1 to DNA. We therefore decided to perform photobleaching FRET experiments as shown in Figure 2. The labeled DNA is photobleached using the 546 nm line of an He-Ne laser on the confocal microscope. Existence of FRET should result in an increase in the fluorescence of GFP-Rae-1. This is never the case, indicating that no FRET occurs between pDNA and GFP-Rae-1. More interestingly, the time evolution of the experiment immediately after the bleach, up to 40 s after (40 s being the total time of acquisition in FRAP experiments of section 3.1) shows no recovery nor for pDNA, neither for Rae-1-GFP, indicating a total failure of mobility of DNA and a total inaccessibility of Rae-1 into these clusters.

4 Discussion

Electropermeabilization has been described in different work as inducing defaults or pores into the plasma membrane of cells. These defaults or pores can be viewed as impermeable obstacles where a membrane protein for example does not have access. If it is the case, apparent mobility of the tracer located into the membrane (in our case the protein RAE-1-GFP), should be affected. Saxton [32, 33] has theoretically studied this problem and shown that apparent diffusion coefficient of the tracers decrease with the fractional

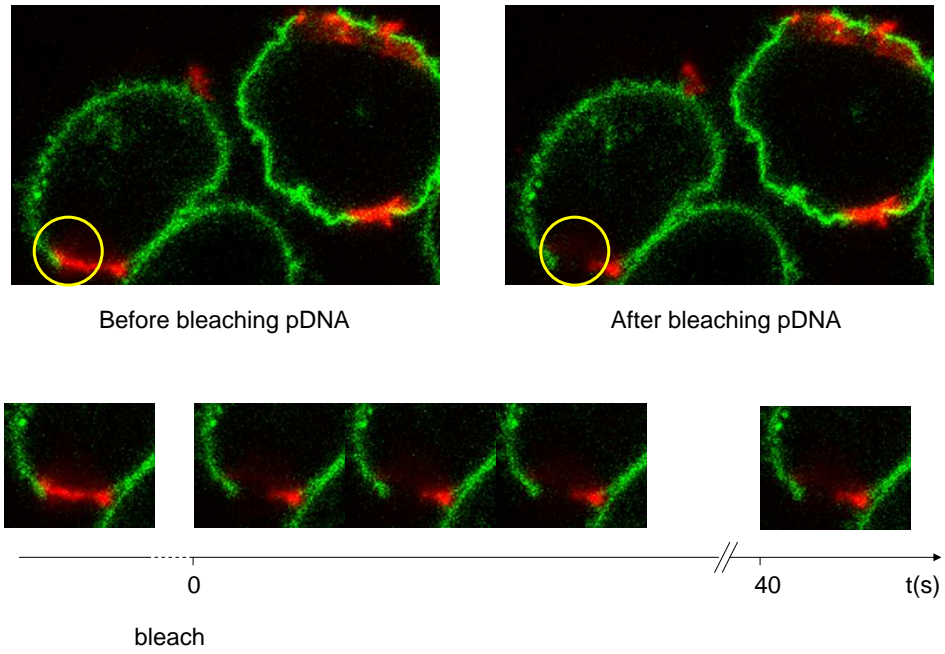


Figure 2:

Photobleaching of plasmid DNA after electrotransfection: Immediately after pDNA photobleaching, fluorescence intensity recovery can be observed with time for both pDNA (in red) and Rae-1 (in green). Both exhibit no recovery, showing the high immobility of the pDNA aggregates in the membrane and showing the incapacity for Rae-1 to enter the aggregate.

area occupied by obstacles, down to zero if obstacles are immobile at a given area (which is the percolation threshold), or more slowly if obstacles are very mobile (as compared to the tracer) meaning that no more percolation threshold exist. In this study, RAE-1 GFP apparent diffusion coefficient is decreased as much as 10% after electroporation. This result is a confirmation of the existence of defects or pores in the outer leaflet of the plasma membrane as it has been shown for several years using other approaches.

4.1 Permeabilized area

According to Saxton's numerical simulations, a decrease of 10% in the apparent diffusion coefficient means that between 10% (in the case of immobile pores or defects) and 20% (in the case of very fast diffusing pores or defects) of the total membrane area of the cell are occupied by these defects or pores. If all these obstacles were fused in a unique one, the aperture angle of this later ($0 < \theta_{ap} < 90^\circ$) will be found between 18° and 26° .

The θ_{ap} value found here can be compared to the values already published in both experimental [15, 16, 34, 35] and numerical simulation works [26]. Portet *et al.* measured the average aperture angle of pores to be 6° by using pDNA translocation into giant unilamellar vesicles (GUVs) made of DOPC. Tekle *et al.* shown that up to 14% of the total membrane surface can be lost when pulsing GUVs made of DOPC, leading to a value of $\theta_{ap} = 22^\circ$. Finally, Gabriel *et al.* measured the average aperture angle as the angle of the extent of the permeabilization immediately after the pulse by visualizing small fluorophore entrance into the cell to be 45° . θ_{ap} values found from these different studies exhibit a high discrepancy. Many factors can account for that discrepancy amongst which the differences in model used (cells [15, 16] or artificial lipid membranes [34, 35]) and differences in external and internal (for artificial lipid membranes) buffers used for electroporation. Nevertheless in [16] the results have been obtained using exactly the same experimental condition than ours (cell type, electroporation buffer and electric field intensity range) and can therefore be directly compared. They exhibit a two-time higher value of θ_{ap} compared as what is found here. This can be explained by two different reasons at least :

- The method used by Gabriel *et al.* reveal the area (or the angle) which is permeant to small molecules such as propidium iodide or ethidium bromide. The continuous pattern of this area can be naively explained by diffusion of the dye 3 ms after the end of the electric pulse (assuming

a diffusion coefficient of $30 \mu m^2.s^{-1}$ in the cytosol shows a mean square displacement of $\langle r^2 \rangle = 0.36 \mu m^2$ after 3ms). If one admit that pores are created during electroporabilization, then, it has been shown that their distribution is spatially discontinuous and that they must be separated at least by a distance equal to their radius [36, 27], which after recalculation lead to a value of $\theta_{ap} = 21^\circ$, close to the one obtained here.

- Our data are acquired one minute after the end of the electric field application. Lifetime distribution of pores or defaults in lipid membrane span a wide range between microseconds up to minutes depending on several factors (field intensity, conductance, lipid membrane composition, artificial vesicles or cells) [6]. Nevertheless, it is clear that the number and/or size of the pores decreases with time after electroporabilization. Since our experiments had to be conducted one minute at least after the end of the pulse, this effect could account for a smaller value of θ_{ap} as compared to the one found in [15, 16]

Alternatively, Krassowska *et al.* [26] performed numerical simulation of the evolution in time and space of pores in a spherical cell exposed to an electric field. They simulated the normalized average area occupied by these pores as a function of the external electric field applied to the cell. In the case of the electric field use in this study ($|E| = 60 kV.m^{-1}$) they found this area to be 0.07% of the total area ($\theta_{ap} = 1.5^\circ$) which is far beyond our experimental results. We have no explanation for such a difference.

4.2 Nature and size of pores or defaults

The mean size of the pores cannot be directly estimated from our study. Nevertheless, the fact that the mobile fraction of RAE-1-GFP is only slightly decreased after electroporabilization gives information about their spatial distribution and their mobility. Since $M \neq 0$ after electroporabilisation, pores or defaults distribution does not induce percolation. If one admit that, after a certain time, the number of pores remains constant then our results can be explained in different ways, i.e., the mean radius of the pores should be in the order of the tracer (Rae-1, $r \sim 1nm$), and/or the mean distance between two pores or defaults must be more than the mean radius of the tracer (to avoid percolation) and/or, finally, if this is not the case, then the pores must be highly mobile (much more than Rae-1 is). Since Rae-1 mobility is also decreased at the equator of the cell (where electric field has no direct effect), we expect the pores to be highly mobile.

4.3 Nature and size of pores or defaults in the presence of pDNA

We have performed the same type of fluorescence recovery after photobleaching experiments in the presence of pDNA, in order to understand the nature of the membrane domains containing pDNA after electroporation. We did not find any striking variation on the mobility of RAE-1-GFP in the presence of pDNA. Here again, this mobility is decreased by 20%, but not more (data not shown). This result was somewhat surprising since many different studies describing pDNA domains at the surface of the cell membrane to be bigger than 200 nm radius [37, 29], that should therefore lead to an increase in the half-time recovery ($t_{1/2}$) and a drastic decrease in the mobile fraction (M) due to RAE-1-GFP molecules trapped in this pDNA domain. Since we were never able to measure this effect, we expect it to be due to the non-contribution in the fluorescence recovery of the trapped molecule in the p-DNA domains. This absence of fluorescence could be of two different origins :

- Energy transfert of Förster type (FRET) between GFP labeling RAE-1 and Cy-5 labeling the pDNA. When very efficient (depending on distance between each molecule, ratio of Cy-5 over GFP), it could lead to total fluorescence extinction of the GFP.
- Total lack of RAE-1 molecules in the pDNA membrane domains.

Performing photobleaching FRET experiments, we have been able to discriminate between these two possibilities. The absence of recovery in the fluorescence of RAE-1 molecules when the Cy-5 molecules are bleached clearly shows that RAE-1-GFP molecules are totally excluded from pDNA domains induced by electroporation. On the other end, as previously described [27], no recovery occurs neither for pDNA fluorescence, showing that the pDNA domains are highly immobile. This result is in favor of a pDNA aggregate that excludes some of the membrane components, if not all, to its periphery, at least in the outer leaflet of the plasma membrane.

References

- [1] E. Neumann, A.E. Sowers, and C.A. Jordan. *Electroporation and Electrofusion in Cell Biology*. 1989.
- [2] D.C. Chang, B.M. Chassy, J.A. Saunders, and A.E. Sowers. *Guide to Electroporation and Electrofusion*. San Diego, 1992.

- [3] JC Weaver. Electroporation: a general phenomenon for manipulating cells and tissues. *J Cell Biochem.*, 51:426–435, 1993.
- [4] J. Gehl. Electroporation: theory and methods, perspectives for drug delivery, gene therapy and research. *Acta Physiologica Scandinavica*, 177(4):437–447, 2003.
- [5] Anita Gothelf, Lluís M Mir, and Julie Gehl. Electrochemotherapy: results of cancer treatment using enhanced delivery of bleomycin by electroporation. *Cancer Treatment Reviews*, 29(5):371 – 387, 2003.
- [6] J. Teissie, M. Golzio, and M.P. Rols. Mechanisms of cell membrane electroporation: A minireview of our present (lack of ?) knowledge. *Biochim. Biophys. Acta - Gen. Subj.*, 1724(3):270 – 280, 2005.
- [7] K. Kinoshita and T. Y. Tsong. Voltage-induced conductance in human erythrocyte membranes. *Biochim Biophys Acta*, 554(2):479–497, 1979.
- [8] I. G. Abidor, L. H. Li, and S. W. Hui. Studies of cell pellets: II. osmotic properties, electroporation, and related phenomena: membrane interactions. *Biophys J*, 67(1):427–435, 1994.
- [9] Mojca Pavlin, Masa Kanduser, Matej Rebersek, Gorazd Pucihar, Francis X Hart, Ratko Magjarevic, and Damijan Miklavcic. Effect of cell electroporation on the conductivity of a cell suspension. *Biophys J*, 88(6):4378–4390, 2005.
- [10] Mojca Pavlin, Vilko Leben, and Damijan Miklavcic. Electroporation in dense cell suspension—theoretical and experimental analysis of ion diffusion and cell permeabilization. *Biochim Biophys Acta*, 1770(1):12–23, 2007.
- [11] S Kakorin, SP Stoylov, and E Neumann. Electro-optics of membrane electroporation in diphenylhexatriene-doped lipid bilayer vesicles. *Biophys. Chem.*, 58(1-2):109–116, 1996.
- [12] T Griesse, S Kakorin, and E Neumann. Conductometric and electrooptic relaxation spectrometry of lipid vesicle electroporation at high fields. *Phys. Chem. Chem. Phys.*, 4(7):1217–1227, 2002.
- [13] R. Benz, F. Beckers, and U. Zimmermann. Reversible electrical breakdown of lipid bilayer membranes: a charge-pulse relaxation study. *J Membr Biol*, 48(2):181–204, Jul 1979.

- [14] M. Hibino, H. Itoh, and K. Kinoshita. Time courses of cell electroporation as revealed by submicrosecond imaging of transmembrane potential. *Biophys J*, 64(6):1789–1800, 1993.
- [15] B. Gabriel and J. Teissié. Direct observation in the millisecond time range of fluorescent molecule asymmetrical interaction with the electroporabilized cell membrane. *Biophys. J.*, 73(5):2630 – 2637, 1997.
- [16] B. Gabriel and J. Teissié. Time courses of mammalian cell electroporabilization observed by millisecond imaging of membrane property changes during the pulse. *Biophys. J.*, 76(4):2158 – 2165, 1999.
- [17] Gorazd Pucihar, Tadej Kotnik, Damijan Miklavich, and Justin Teissié. Kinetics of transmembrane transport of small molecules into electroporabilized cells. *Biophysical Journal*, 95(6):2837 – 2848, 2008.
- [18] Marie-Pierre Rols and Justin Teissié. Electroporabilization of mammalian cells to macromolecules: Control by pulse duration. *Biophysical Journal*, 75(3):1415 – 1423, 1998.
- [19] LM Mir, H Banoun, and C Paoletti. Introduction of definite amounts of nonpermeant molecules into living cells after electroporabilization - direct access to the cytosol. *Exp. Cell Res.*, 175(1):15–25, 1988.
- [20] E. Tekle, R. D. Astumian, and P. B. Chock. Selective and asymmetric molecular transport across electroporated cell membranes. *Proc Natl Acad Sci U S A*, 91(24):11512–11516, 1994.
- [21] M. R. Prausnitz, C. D. Milano, J. A. Gimm, R. Langer, and J. C. Weaver. Quantitative study of molecular transport due to electroporation: uptake of bovine serum albumin by erythrocyte ghosts. *Biophys J*, 66(5):1522–1530, 1994.
- [22] M. R. Prausnitz, J. D. Corbett, J. A. Gimm, D. E. Golan, R. Langer, and J. C. Weaver. Millisecond measurement of transport during and after an electroporation pulse. *Biophys J*, 68(5):1864–1870, 1995.
- [23] Zachary A Levine and P. Thomas Vernier. Life cycle of an electropore: field-dependent and field-independent steps in pore creation and annihilation. *J Membr Biol*, 236(1):27–36, Jul 2010.
- [24] Mounir Tarek. Membrane electroporation: a molecular dynamics simulation. *Biophys J*, 88(6):4045–4053, Jun 2005.

- [25] D. Peter Tieleman. The molecular basis of electroporation. *BMC Biochem*, 5:10, Jul 2004.
- [26] W. Krassowska and P. D. Filev. Modeling electroporation in a single cell. *Biophys. J.*, 92(2):404 – 417, 2007.
- [27] Jean-Michel Escoffre, Thomas Portet, Cyril Favard, Justin Teissie, David S. Dean, and Marie-Pierre Rols. Electromediated formation of DNA complexes with cell membranes and its consequences for gene delivery. *Biochim. Biophys. Acta-Biomembranes*, 1808(6):1538–1543, 2011.
- [28] VA Parsegian. Energy of an ion crossing of a low dielectric membrane: Solutions to four relevant electrostatic problems. *Nature*, 221:844–846, 1969.
- [29] E Phez, C Faurie, M Golzio, J Teissie, and MP Rols. New insights in the visualization of membrane permeabilization and DNA/membrane interaction of cells submitted to electric pulses. *Biochim. Biophys. Acta-Gen. Subj.*, 1724(3):248–254, 2005.
- [30] D Axelrod, DE Koppel, J Schlessinger, E Elson, and WW Webb. Mobility measurement by analysis of fluorescence photobleaching recovery kinetics. *Biophys. J.*, 16(9):1055–1069, 1976.
- [31] C. Matthews and C. Favard. Theory, principles and applications of fluorescent technologies in cellular biology and cancer research. *Bull. Cancer (French)*, 94(1):115–125, 2007.
- [32] MJ Saxton. Lateral diffusion in an archipelago - Effects of impermeable patches on diffusion in a cell-membrane. *Biophys. J.*, 39(2):165–173, 1982.
- [33] MJ Saxton. Lateral diffusion in an archipelago - The effect of mobile obstacles. *Biophys. J.*, 52(6):989–997, 1987.
- [34] E Tekle, RD Astumian, WA Friauf, and PB Chock. Asymmetric pore distribution and loss of membrane lipid in electroporated DOPC vesicles. *Biophys. J.*, 81(2):960–968, 2001.
- [35] Thomas Portet, Cyril Favard, Justin Teissie, David S. Dean, and Marie-Pierre Rols. Insights into the mechanisms of electromediated gene delivery and application to the loading of giant vesicles with negatively charged macromolecules. *Soft Matter*, 7(8):3872–3881, 2011.

- [36] M Winterhalter and W Helfrich. Effect Of Voltage On Pores In Membranes. *Phys. Rev. A*, 36(12):5874–5876, 1987.
- [37] Muriel Golzio, Justin Teissie, and Marie-Pierre Rols. Direct visualization at the single-cell level of electrically mediated gene delivery. *Proc Natl Acad Sci U S A*, 99(3):1292–1297, Feb 2002.